

## Flow Dynamics in Eccentrically Rotating Flasks Used for Dispersant Effectiveness Testing

VIKRAM J. KAKU<sup>a</sup>, MICHEL C. BOUFADEL<sup>b,\*</sup>,  
ALBERT D. VENOSA<sup>c</sup> and JAMES WEAVER<sup>d</sup>

<sup>a</sup>*Department of Mechanical Engineering, Temple University, 1947 N. 12th Street,  
Philadelphia, PA 19122, USA*

<sup>b</sup>*Department of Civil & Environmental Engineering, Temple University, 1947 N. 12th  
Street, Philadelphia, PA 19122, USA*

<sup>c</sup>*Oil Spill Research Program, U.S. Environmental Protection Agency, National Risk  
Management Research Laboratory, 26 W. Martin Luther King Drive, Cincinnati, OH  
45268, USA*

<sup>d</sup>*U.S. Environmental Protection Agency, National Exposure Research Laboratory, 960  
College Station Road, Athens, GA 30605, USA*

Received 28 October 2005; accepted in revised form 1 February 2006

**Abstract.** The evaluation of dispersant effectiveness used for oil spills is commonly done using tests conducted in laboratory flasks. We used a Hot Wire Anemometer (HWA) to characterize mixing dynamics in the Swirling Flask (SF) and the Baffled Flask (BF), the latter is being considered by the EPA to replace the prior to test dispersant effectiveness in the laboratory. Five rotation speeds of the orbital shaker carrying the flasks were considered,  $\Omega = 50, 100, 150, 175$  and  $200$  rpm. The radial and azimuthal water speeds were measured for each  $\Omega$ . It was found that the flow in the SF is, in general, two-dimensional changing from horizontal at low  $\Omega$  to axi-symmetric at high  $\Omega$ . The flow in the BF appeared to be three-dimensional at all rotation speeds. This indicates that the BF is more suitable for representing the (inherently) 3-D flow at sea. In the SF, the speeds and energy dissipation rates  $\varepsilon$  increased gradually as the rotation speed increased. Those in the BF increased sharply at rotation speeds greater than  $150$  rpm. At  $200$  rpm, the Kolmogorov scale (i.e., size of smallest eddies) was about  $250$  and  $50 \mu\text{m}$  in the SF and BF, respectively. Noting that the observed droplet sizes of dispersed oils range from  $50$  to  $400 \mu\text{m}$  (hence most of it is less than  $250 \mu\text{m}$ ), one concludes that the mixing in the SF (even at  $200$  rpm) is not representative of the vigorous mixing occurring at sea.

**Key words:** anemometers, data acquisition, eccentric, energy dissipation, oil spills, rotating flasks, time series analysis, turbulence, velocity gradient

---

\*Corresponding author, E-mail: boufadel@temple.edu

**Nomenclature**

$A$	a constant of order one
$f$	frequency of velocity fluctuations, $s^{-1}$
$G$	local velocity gradient, $s^{-1}$
$k$	wavenumber, $m^{-1}$
$L$	integral length scale, m
$R_E$	autocorrelation coefficient function
$\bar{U}_i$	time-averaged (mean) velocity
$u_i$	instantaneous velocity
$u'_i$	randomly fluctuating velocity
$\tilde{u}_i$	regular oscillatory component of velocity

**Greek Symbols**

$\varepsilon$	local energy dissipation rate, $m^2/s^3$
$\bar{\varepsilon}$	flask average energy dissipation rate, $m^2/s^3$
$\eta$	local Kolmogorov microscale, $\mu m$
$\bar{\eta}$	flask average Kolmogorov scale, $\mu m$
$\nu$	kinematic viscosity, $m^2/s$
$\Omega$	orbital shaker speed, rpm
$\tau$	time lag, sec
$\tau_{E_i}$	integral time scale, sec

**1. Introduction**

The adverse effects of oil spills are more severe when the slicks reach the shoreline. For this reason, much effort is placed on mitigating the spills offshore. In agitated seas, a promising approach is to apply chemicals known as dispersants on the oil slick that cause the slick to break into droplets that penetrate deep in the sea due to the action of waves. This process is termed in the oil literature as dispersion (to be distinguished from the spreading of chemicals due to the spatial variation of velocity such as presented by Taylor [1, 2], Fischer *et al.* [3]). Dispersion of oil is a chemico-physical process that depends both on the type of dispersant/oil pair and on the sea state. The dispersed oil droplets get carried away from the contaminated area due to prevailing currents, and eventually adhere to suspended particulate matter and/or biodegrade [4, p. 3].

Various field studies and laboratory experiments have been conducted to evaluate the effectiveness of dispersants under various sea conditions. Field studies are accompanied by experimental uncertainties in the sea; replicates are usually difficult to achieve due to constantly changing climatic conditions and for economic reasons. Hence, smaller scale testing is extensively used to study dispersant effectiveness. Examples of commonly used tests include the Swirling flask (SF) test method [4–7], the Warren Spring Laboratory (WSL) test method [7–11], and the Exxon dispersant effectiveness test method [12–14].

The Swirling Flask (SF) (Figure 1a) test consists of placing a mixture of oil, seawater, and a dispersant in the SF positioned on an orbital (circular motion) shaker [4], then mixing the contents for a specified amount of time, allowing a short settling time, and then extracting the contents from the SF and measuring the concentration of oil dispersed in the water. The claimed advantages of this test are its ease of use and simplicity.

The U.S. Environmental Protection Agency (EPA) is considering adopting a new flask, the Baffled Flask (BF), in a context of a new (improved) testing protocol for dispersants. The BF has four baffles in it (Figure 1b) that induce three-dimensional motion. The rationale for the selection of the BF along with the regulatory aspect of dispersant effectiveness are thoroughly addressed by Sorial *et al.* [15, 16] and references therein. Chandrasekar *et al.* [17] evaluated dispersant effectiveness in the BF under various simulated environmental conditions.

This study focuses on the hydrodynamics of the BF for conducting dispersant testing. Although one rotation speed is used in the standard flask test (150 rpm for the SF test and 200 rpm for the BF test), we selected five rotation speeds to better understand the mixing characteristics in both

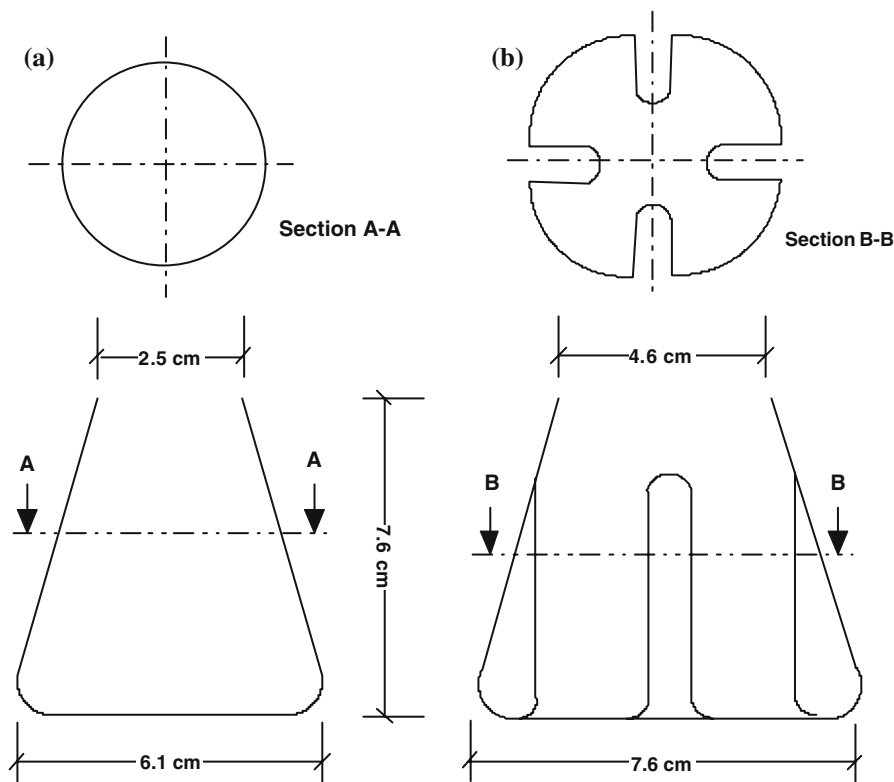


Figure 1. Schematic cross-section of (a) the Swirling Flask (b) the Baffled Flask.

flasks. It is understandable that these rotation speeds could be related to various sea states. But such a linkage is left for future work.

The five rotation speeds were  $\Omega = 50, 100, 150, 175,$  and  $200$  rpm. A Hot Wire Anemometer (HWA) was used to measure the instantaneous water velocity distributions in the flasks. These measurements were then used to evaluate the overall hydraulics in the flasks, and to compute turbulence quantities, such as the energy dissipation rate per unit mass,  $\varepsilon$  and the Kolmogorov scale,  $\eta$ .

## 2. Theory

As dispersion of oil into fine oil droplets takes place at the smaller scale (i.e., below the 1-cm scale), simulation of these interactions in laboratory experiments is possible because the smallest eddies in the flask are similar to those at sea due to the fact that the small-scale structure of turbulence is universal (i.e. independent of the system) [18, 19]. This means that the energy dissipation rate per unit mass,  $\varepsilon$ , can be used as an appropriate scaling parameter [20]. The units of  $\varepsilon$  are watts/kg, but  $\varepsilon$  is commonly expressed as  $\text{m}^2/\text{s}^3$  in the oceanography literature.

The dissipation of kinetic energy occurs due to laminar and turbulent shears within the water. The shear is directly proportional to velocity gradients, which play an important role in the mixing of chemicals, such as oil and dispersant. A well-known relation exist between the local  $\varepsilon$  and the local absolute velocity gradient  $G(\text{s}^{-1})$  at every location in the fluid [21, 22]:

$$\varepsilon = \nu G^2, \quad (1)$$

where  $\nu$  is the kinematic viscosity of water ( $10^{-6} \text{m}^2/\text{s}$  at  $20^\circ\text{C}$ ). Hence, knowledge of  $\varepsilon$  is equivalent to knowledge of velocity gradient. Alternatively, one may use velocity measurements in a selected water body to compute the velocity gradient, and subsequently the energy dissipation rate. This is the approach that we adopt in this work to evaluate average energy dissipation rates in the SF and the BF. We hypothesize, as commonly done in most environmental flows [23, 24], that the energy dissipation occurs predominantly due to turbulent shear, and that the laminar shear can be neglected. For this reason, we present the methodology for evaluating energy dissipation rates based on turbulence theory.

In turbulent mixing, large eddies carry the energy obtained from the general motion of the fluid [25, 26]. These eddies break into smaller eddies, which in turn break into smaller eddies down to a scale where molecular viscosity effects become dominant. As hypothesized by Kolmogorov [27], there is a cascade of kinetic energy from the large eddies to smaller one down to the so-called Kolmogorov scale (less than a millimeter in this

work) where the kinetic energy is dissipated by viscous forces due to friction of water molecules on each other.

The small-scale structure of turbulence tends to be independent of any orientation effects, and is thus locally isotropic. In isotropic turbulence, the dissipation rate per unit mass is simplified to [22]:

$$\varepsilon = 15\nu \overline{\left(\frac{\partial u_i}{\partial i}\right)^2}, \quad (2)$$

where  $u_i$  ( $i = x, y, z$ ) is the instantaneous velocity in any “ $i$ ” direction, and the overbar indicates temporal average. The mixing due to turbulence is much larger than that due to the spatial variation of the velocity (i.e., the mean gradient of velocity). For this reason, only the turbulence contribution is considered in the evaluation of  $\varepsilon$  [28–30]. Considering the orbital motion of the flask, one may write:

$$u_i(s, t) = (\overline{U}_i(s) + \tilde{u}_i(s, t)) + u'_i(s, t); \quad i = x, y, z, \quad (3)$$

where  $\overline{U}_i$  is the time-averaged (mean) velocity that depends solely on location,  $\tilde{u}_i$  is the oscillatory component due to the oscillatory motion of the flask (it depends on both location in the flask and time), and  $u'_i$  is the component due to turbulence. The oscillatory component,  $\tilde{u}_i$ , could be obtained as a moving average of the time series of  $u_i$  (essentially a smooth line that would exist even in the absence of turbulence).

The evaluation of  $\varepsilon$  in this work is done using the autocorrelation function approach [29, 31]. The energy dissipation rate per unit mass may be written as:

$$\varepsilon = A \frac{(u'_{\text{rms}})^2}{\tau_{E_i}}, \quad (4)$$

where  $u'_{\text{rms}}$  is the root mean square (RMS) value of the turbulent component of velocity,  $A$  is a constant of order unity, and  $\tau_{E_i}$  is the integral time scale of the velocity in the direction “ $i$ ”:

$$\tau_{E_i} = \int_0^\infty R_{E_i} dt, \quad (5)$$

where  $R_{E_i}$  is the temporal autocorrelation function, viz:

$$R_{E_i} = \frac{\overline{u'_i(t)u'_i(t+\tau)}}{(u'_i)^2}, \quad (6)$$

where  $\tau$  is the time lag. Note that  $R_{E_i}$  is assumed the same in all directions, a direct consequence of the isotropic turbulence assumption. In practice an

upper limit of  $\infty$  is impractical in Equation (5), so the point of first zero crossing of the autocorrelation function is used [32].

The Kolmogorov scale,  $\eta$ , provides an estimate of the smallest eddy that can exist prior to the dissipation by (molecular) viscous friction. It is estimated based on dimensional arguments [22] as:

$$\eta = \left( \frac{v^3}{\varepsilon} \right)^{1/4}, \quad (7)$$

The spectrum of velocity in turbulent flows has the following property [18]:

$$E \propto k^{-5/3}, \quad (8)$$

where  $k$  is the wave number (inverse of length). For a time series of measurements at a point, a turbulent flow has the following spectrum [33]:

$$E \propto f^{-2}, \quad (9)$$

where  $f$  represents the frequency of velocity fluctuations. Equation (9) is valid in situations where Taylor's "frozen turbulence" hypothesis is applicable [26, 34]. The hypothesis stipulates that turbulent eddies are advected without a change in their statistical properties, allowing therefore to infer these properties from a time series at a point.

### 3. Experimental Set-Up

The experimental setup (Figure 2) consisted of 150-ml Swirling Flask (SF), 200-ml baffled trypsinizing flask (BF), and an orbital shaker (Model #3518, Lab-Line Instruments Inc.). Each flask contained 120 ml of tap water as the working fluid. The flasks were held in place on the orbital shaker using flask holders. The shaker has an orbital diameter of 1.9 cm. During rotation, the location of the flasks was measured using a Position Transducer (PN150-0121, SpaceAge Control Inc.). A Hot Wire Anemometer (HWA) (TSI 1210-20W, with single cylindrical sensor) was mounted on the orbital shaker to measure the water speed in the flasks in two horizontal directions, radial and azimuthal. The radial direction was along the radius of the flask while the azimuthal direction was tangential to the wall of flask and normal to radial direction. The HWA was moving with the orbital shaker and flask, such that the HWA readings are of water speed. Location and speed measurements were interfaced to a computer using a data-acquisition board, DAS 1401, by Keithley Instruments Inc., (Cleveland, Ohio) with a built-in analog-to-digital circuit. The data logging software LABTECH Notebook Pro (Laboratory Technologies, Inc.) was used. Figure 2 is a schematic of the experimental setup.

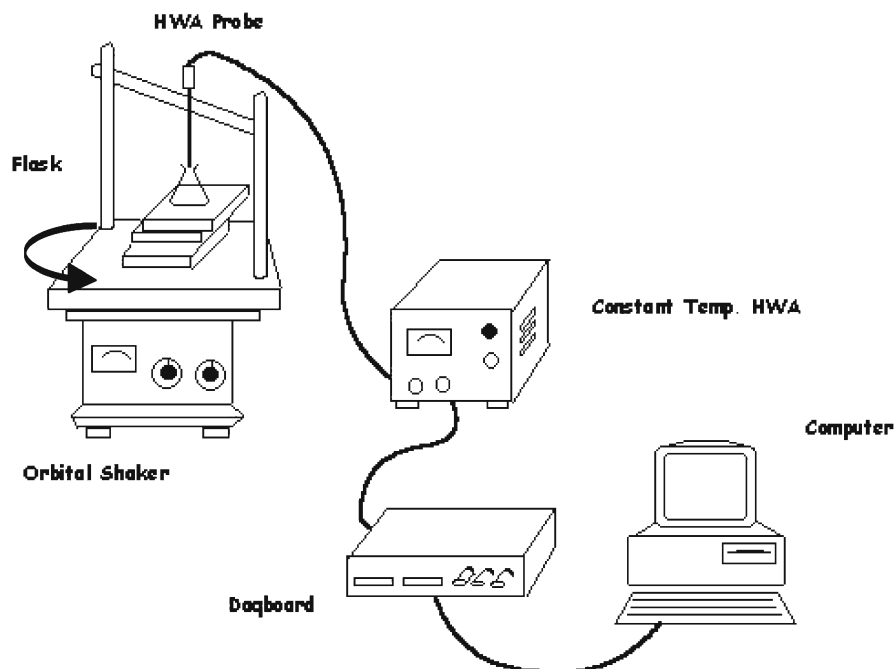


Figure 2. Schematic of the experimental setup.

The HWA is essentially an electric resistor that cools upon passage of water flow. The change in temperature alters the voltage that passes through the resistor. Hence, voltage reading across the HWA provides a surrogate measure of the water velocity. The HWA was calibrated in the velocity range (0–50 cm/s). The output voltage from HWA at zero velocities fluctuated from 2.8 to 2.85 volts throughout the duration of the experiments. Hence, the uncertainty in measurements is expected to be less than 4%. More information on the calibration procedure can be found in Kaku *et al.* [35].

The velocities were measured in the center vertical plane of both the flasks at a spatial interval of 2 mm in the horizontal (i.e. radial) direction and 5 mm in the vertical direction. This totaled to 70 locations in the SF and 80 locations in the BF. The data collection frequency was 1000 Hz, but the response of the whole setup was estimated at about 400 Hz, above which noise overpowered the signal (discussed below). The sampling duration was 10 seconds for each velocity component. This resulted in a time series of 10,000 measurements for each component. Although one flask rotation took about 1.2 second at  $\Omega = 50$  rpm and 0.3 second at  $\Omega = 200$  rpm, the long measurement duration (10 seconds) was intended to increase the reliability of the experiments by having enough replicates: 8 replicates at 50 rpm and 33 replicates at 200 rpm. The increase in the

number of replicates with the rotation speed is a welcome outcome, as the flow becomes more random with an increase in  $\Omega$ , and a large number of replicates minimizes sampling errors.

## 4. Results

### 4.1. AVERAGE SPEEDS

For each rotation speed of the orbital shaker, the average radial and azimuthal water speeds,  $|\overline{U}_i|$  ( $i = x, z$  in Equation 3) were computed by taking the average over 10 seconds of the time series at the measurement location. The speed of water (i.e., magnitude of velocity) is used because it was not possible to ascertain the sense of the radial velocities. The sense of the azimuthal velocity is known because the direction of rotation is known. Figures 3 and 4 report contours of the speeds in the SF and BF, respectively.

Both the radial and azimuthal speeds in the SF (Figure 3) appear to be symmetric (within experimental errors) with respect to the center axis. These speeds are also stratified at rotation speeds  $\Omega \leq 150$  rpm, with the largest speed values occurring near the surface. For  $\Omega > 150$  rpm, a zone of relatively low speed occupies the central portion of the flask. One could talk loosely of a “stagnant core” in the SF at  $\Omega = 175$  and 200 rpm. The flow in the SF appears to be quasi-two-dimensional at the extreme values of  $\Omega$ , switching from horizontal at low  $\Omega$  to axi-symmetric at high  $\Omega$ .

The radial speed contours of the BF (Figure 4, left panel) show that the zone of high speed remains essentially in the center portion of the flask, moving downward as  $\Omega$  increases. For the azimuthal speed in the BF (Figure 4, right panel) one notes that as the rotation speed increased, the high speed values moved from the high center portion to the lower outer portions of the BF.

For each flask, the radial and azimuthal speeds seem to be comparable for the same  $\Omega$ . At  $\Omega = 50$  rpm, the speeds in both flasks were comparable, but the difference between speeds in flasks increases with the rotation speed. At  $\Omega = 200$  rpm, the maximum absolute values of speed (i.e.,  $\max |\overline{U}_i|$ ) are 16 and 60 cm/s, in the SF and BF, respectively.

For each  $\Omega$ , the flask-averaged radial and azimuthal speed were obtained by averaging the values reported in Figures 3 and 4. Figure 5 reports these averages as function of  $\Omega$ . The BF plots show a sudden increase for  $\Omega \geq 150$  rpm. This is probably because a fully turbulent regime was reached around those rotation speed values. This is further addressed in the Discussion Section. For the SF plots, the azimuthal speed of the SF became double the radial at  $\Omega = 200$  rpm, but the values were relatively small. Figure 5 clearly shows that the water speeds in the BF are much higher than those in the SF for  $\Omega \geq 100$  rpm.

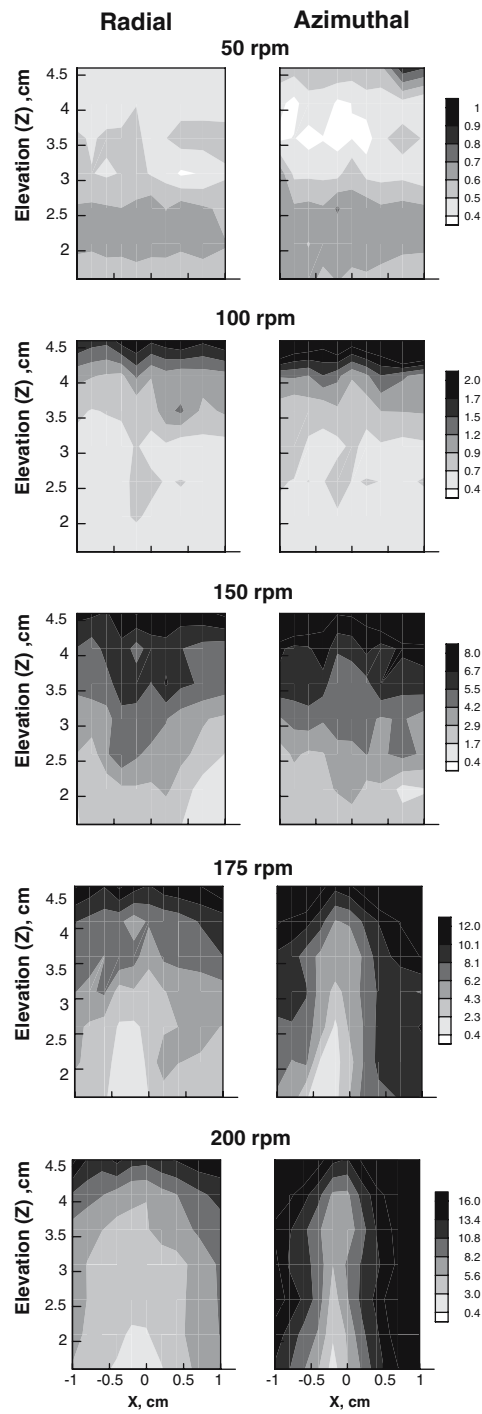


Figure 3. Contours of the average (left) radial and (right) azimuthal velocities in the SF for five rotation speeds of the orbital shaker; 50, 100, 150, 175, and 200 rpm.

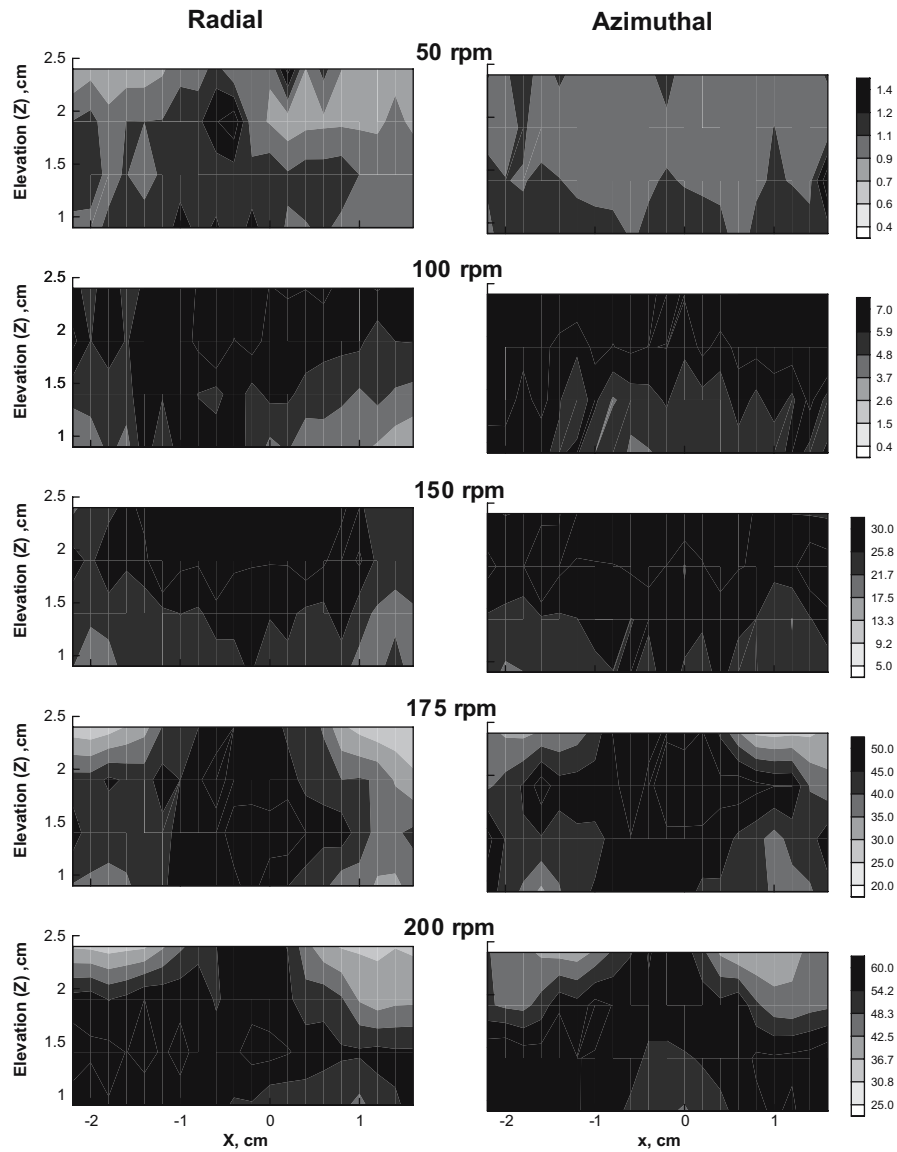


Figure 4. Contours of the average (left) radial and (right) azimuthal velocities in the BF for five rotation speeds of the orbital shaker; 50, 100, 150, 175, and 200 rpm.

#### 4.2. SPECTRA

Figures 6 and 7 contain plots of the natural logarithm of the Fourier spectrum as function of the natural logarithm of frequencies. The spectra were computed by averaging the spectral amplitudes at all locations corresponding to the same frequencies. The figures also show the theoretical  $-2$

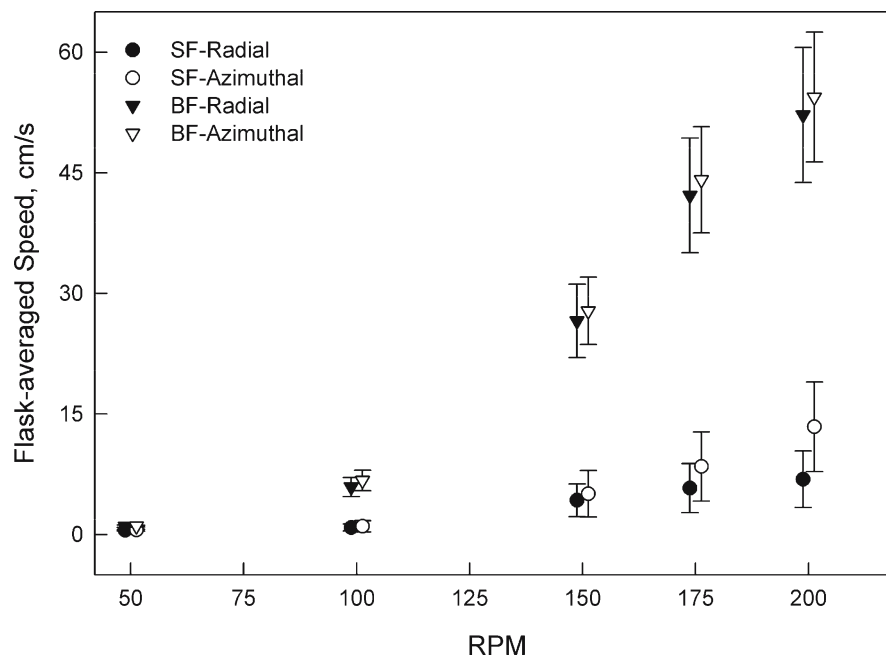


Figure 5. Variation of the average radial and azimuthal speeds as function of the rotation speed for both flasks.

slope based on Kolmogorov theory (Equation 9). The observed spectra displayed periodicity, which is to be expected due to the periodic nature of the motion. The highest peak occurred at the frequency of rotation. The peaks that followed occurred at multiple frequencies of the main one. The periodicity could be removed from the velocity field only if an analytical solution for the average velocity  $\tilde{u}$  is available, as done in the work of Kitaigorodskii *et al.* [36] while evaluating turbulence behavior below waves.

The similarity between the radial and azimuthal spectra indicated that the assumption of isotropic turbulence was valid. The peaks of the spectra in the BF were higher than that in the SF, indicating higher kinetic energy in the BF system. For both flasks, the peaks of the spectra increased with the rpm, indicating that there is an increase in energy dissipation of the system with the increase in orbital speed, an expected result.

For all spectra, one could stipulate the existence of a scaling regime (straight line behavior) whose range increases with the rotation speed of the shaker. The flattening of the spectra at high frequencies is due to dominance of noise, especially at low  $\Omega$  values. But as  $\Omega$  increased, the range of scaling increased to encompass frequencies that were dominated by noise at lower  $\Omega$ . At the maximum rotation speed (i.e, 200 rpm), noise appears to be present only at frequencies larger than 400 Hz.

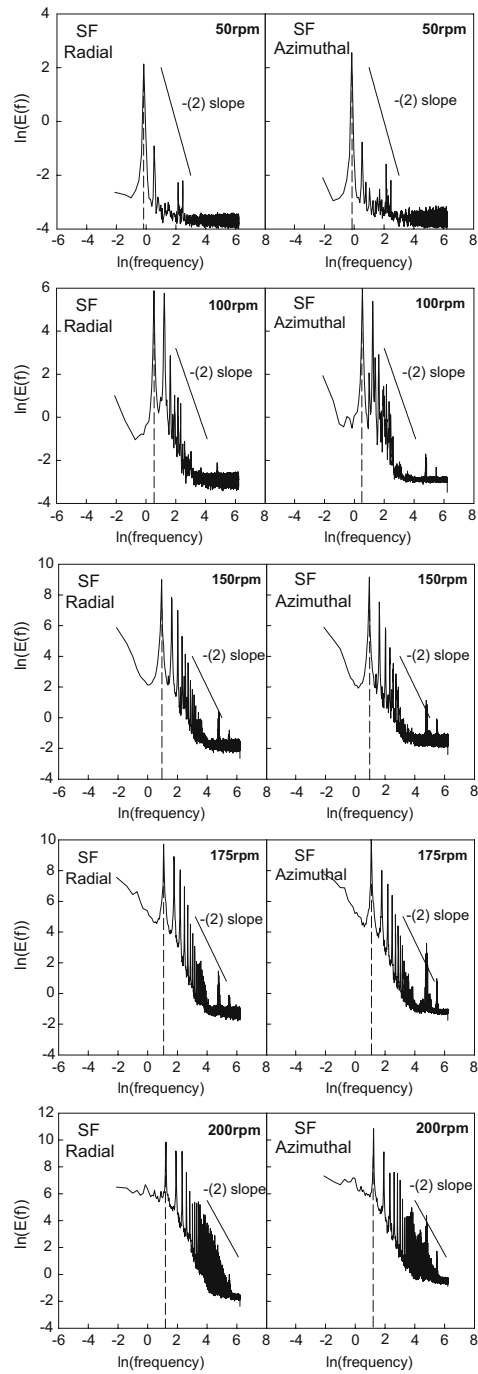


Figure 6. Spectra of radial and azimuthal velocities in the SF for all rotation speeds. The peak on the dashed line shows orbital shaker frequency of  $\Omega/60$  Hz, where  $\Omega$  is the rotation speed expressed in rpm.

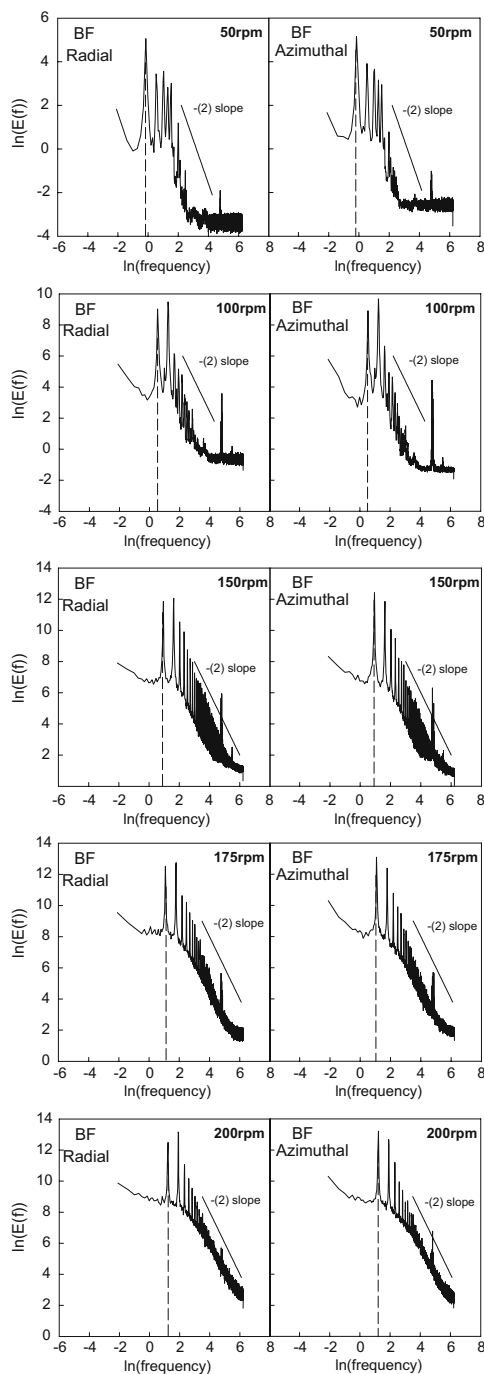


Figure 7. Spectra of radial and azimuthal velocities in the SF for all rotation speeds. The peak on the dashed line shows orbital shaker frequency of  $\Omega/60$  Hz, where  $\Omega$  is the rotation speed expressed in rpm.

Figure 7 indicates that the spectra of the Baffled Flask at 150 rpm resemble those of the 175 and 200 rpm. However, the spectra of the 100 rpm resemble more those of the 50 rpm. This could indicate that a fully developed turbulent regime is reached at  $\Omega = 150$  rpm and increasing the rotation speed does not greatly increase the range of scaling.

#### 4.3. ENERGY DISSIPATION

The energy dissipation rate,  $\varepsilon$ , was estimated at each measurement location using Equation (4) with the coefficient “ $A$ ” set equal to 1.0. The integral time scale (Equation 5) was evaluated at each measurement location by integrating from time zero to the time of the first zero crossing of the auto-correlation function. The Simpson’s method was used [37] for the numerical integration. One value of  $\varepsilon$  was computed for each velocity component. The average of these two values was then obtained, and it was considered as representative of the energy dissipation at that location. Figures 8 and 9 report the decimal logarithm of  $\varepsilon$  for the SF and BF, respectively. These figures should be compared to the corresponding average velocity figures, Figures 3 and 4. In general, higher energy dissipation in Figures 8 and 9 occurred at locations where  $|\bar{U}_i|$  ( $i = x, z$ , Equation 3) is high (Figures 3 and 4). The values of  $\varepsilon$  in the SF were higher at the surface and decreased rapidly with depth. The values of  $\varepsilon$  in the BF were much higher at the edges, most likely due to the presence of baffles.

The flask-averaged dissipation rate,  $\bar{\varepsilon}$ , was computed for both flasks at each rotation speed. It is reported in Figure 10 as function of  $\Omega$ . For the BF,  $\bar{\varepsilon}$  increased by about three orders of magnitude for  $\Omega$  increasing from 50 to 200 rpm (a logarithmic representation on the ordinate axis was needed for clarity of presentation). The  $\bar{\varepsilon}$  values for the SF increased by approximately one order of magnitude. The maximum  $\bar{\varepsilon}$  value for the SF (i.e., at 200 rpm) is about an order of magnitude smaller than that of the BF at 150 rpm.

#### 4.4. THE KOLMOGOROV SCALE

The Kolmogorov scale was computed in the flasks according to Equation (7), assuming the water at 20 °C. Hence, two values were obtained at each measurement point, one in each direction. The local  $\eta$  value was obtained as the average of the two values. The flask-averaged Kolmogorov scale,  $\bar{\eta}$ , was obtained by taking the arithmetic average of the local  $\eta$  values. Figure 11 shows, expectedly, that  $\bar{\eta}$  decreases with  $\Omega$ . The decrease of  $\bar{\eta}$  is sharp initially, but becomes milder for  $\Omega \geq 150$  rpm. At  $\Omega = 200$  rpm,  $\bar{\eta} = 250 \mu\text{m}$  and  $50 \mu\text{m}$ , for the SF and BF, respectively.

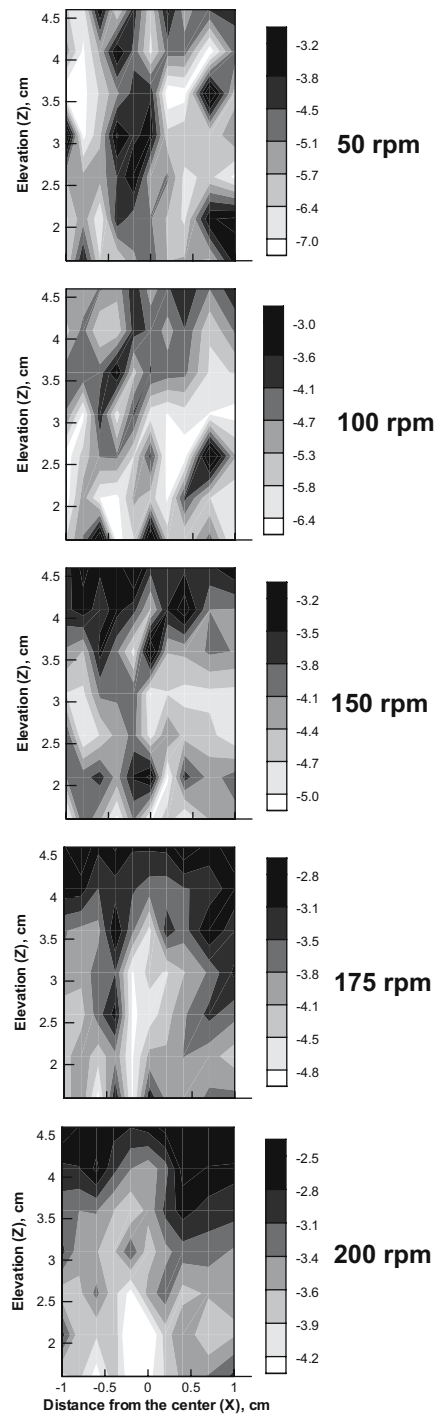


Figure 8. Contour plots of  $\log(\epsilon)$  in the SF for all rotation speeds. Label represents values of  $\log(\epsilon)$ .

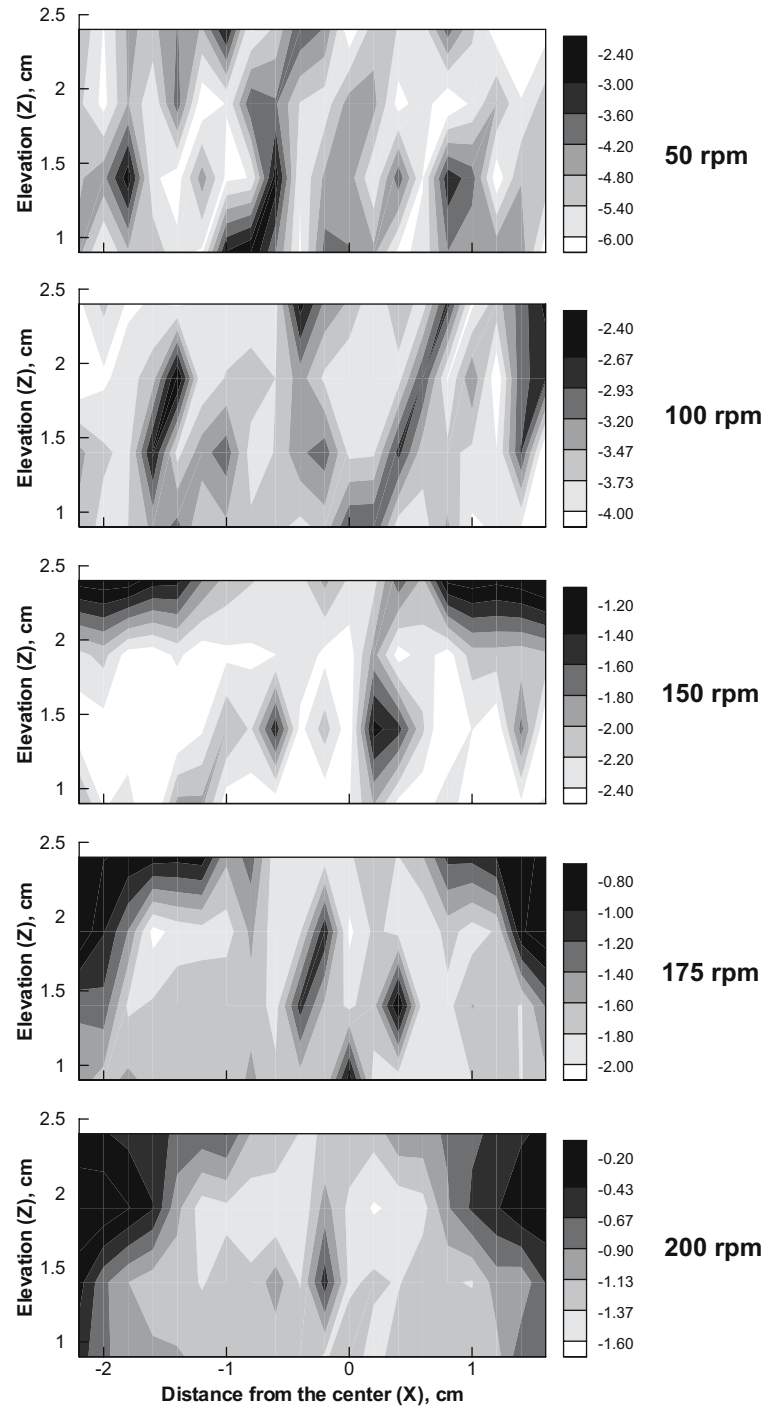


Figure 9. Contour plots of  $\log(\epsilon)$  in the BF for all rotation speeds. Label represents values of  $\log(\epsilon)$ .

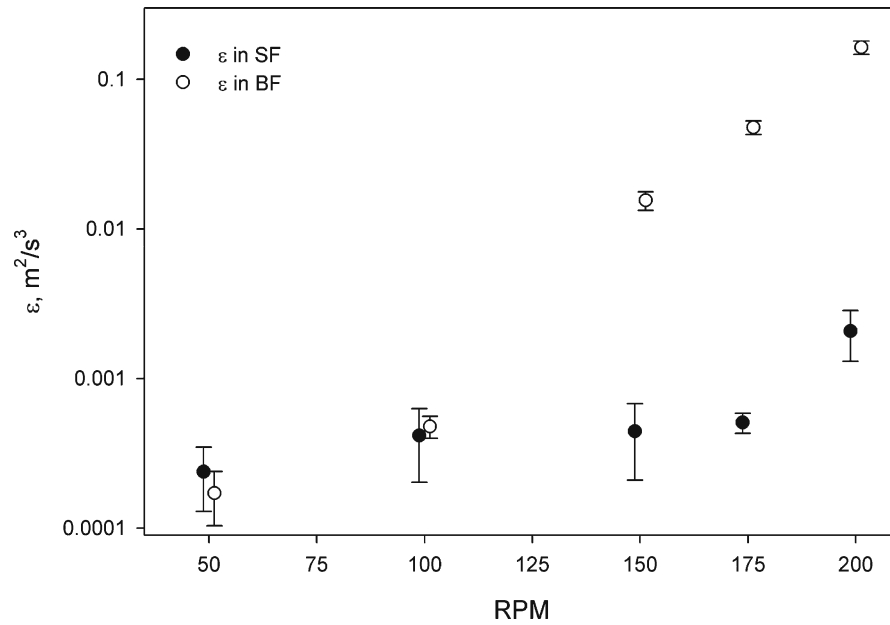


Figure 10. Variation of  $\log(\epsilon)$  in the SF and the BF as function of the rotation speed.

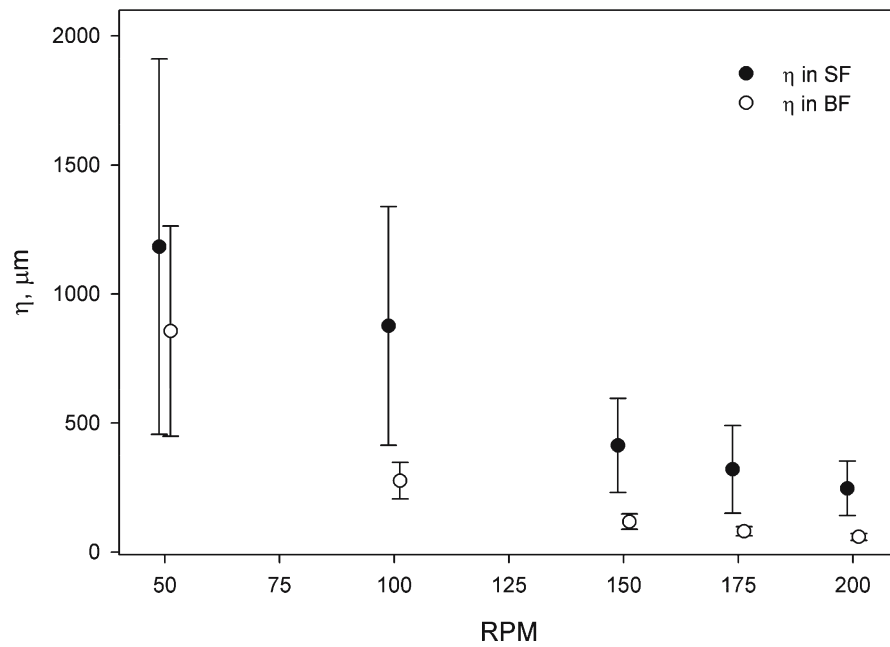


Figure 11. Variation of the Kolmogorov scale in the SF and the BF as function of the rotation speed.

## 5. Discussion

The value of the Kolmogorov scale,  $\bar{\eta}$ , represents the size of the smallest eddies. If the smallest eddies are larger than the oil droplets, they tend to entrain oil droplets within them without breaking them. However, if the smallest eddies are smaller than an oil droplet, they would stretch it between them causing it to break. The size distribution of dispersed oil at sea was observed to range from 50 to 400  $\mu\text{m}$  [8, 10, 20, 38, 39]. The value of  $\bar{\eta}$  in the SF at 150 rpm was about 400  $\mu\text{m}$ . This implies that the mixing in the SF at 150 rpm does not theoretically create a high number of oil droplets whose sizes are smaller than 400  $\mu\text{m}$ . This discrepancy indicates that there might be theoretical objections to using the mixing in the SF at 150 rpm to represent the mixing at sea. The average Kolmogorov scale in the BF at 200 rpm was about 50  $\mu\text{m}$ , which should cause breakup of oil droplets approaching that scale.

Evidently, increasing the rotation speed of the SF would result in a decrease in the Kolmogorov scale, as noted in Figure 11. However, there are logistic limitations to increasing the speed. First, note that  $\eta$  is inversely proportional to  $\varepsilon$  to the power 1/4. Second, our own calculations showed that an increase by 50 rpm over the speed of 150 rpm resulted in a decrease in  $\eta$  to only 250  $\mu\text{m}$  from 400  $\mu\text{m}$ . Hence, the sought 50  $\mu\text{m}$  in  $\bar{\eta}$  might require a rotational speed as high as 1000 rpm.

Figure 7 indicates that the spectra of the BF at 150 rpm resemble those of the 175 and 200 rpm. However, the spectra of the 100 rpm resemble more those of the 50 rpm. This could indicate that a fully developed turbulent regime is reached at  $\Omega = 150$  rpm, and increasing the rotation speed does not greatly increase the range of scaling. This is further confirmed by the fact that the Kolmogorov scale in the BF did not decrease greatly going from 150 to 200 rpm (Figure 11).

We believe that the use of an average energy dissipation rate  $\bar{\varepsilon}$  is more physical than using an average shear rate  $\bar{G}$  due to the fact that  $\varepsilon$  represents an energy rate, while  $G$  represents a velocity gradient. Hence,  $\bar{\varepsilon}$  could be stipulated based on the law of conservation of energy. There is no counterpart for  $G$  (i.e., there is no law that requires the conservation of velocity or its gradient).

By accepting the conservation of  $\varepsilon$  as a necessary condition for replicating the mixing at sea, it is important to know the sea state corresponding to the values that we found in this study. Terray *et al.* [40] conducted velocity measurements in the top two meters of Lake Ontario and found  $\varepsilon$  to vary between  $10^{-5}$  and  $10^{-2} \text{m}^2/\text{s}^3$ . The significant wave height in that study was about 0.25 m. Drennan *et al.* [41] conducted similar measurements in the Atlantic Ocean off of the Maryland Coast. They found  $\varepsilon$  varying between  $10^{-4}$  and  $5.0 \times 10^{-4} \text{m}^2/\text{s}^3$ . The significant wave height was

about 1.0 m. These values are smaller than those reported by Terray *et al.* [40] despite the fact that the wave height was four times larger. However, as discussed by Drennan *et al.* [41], the measurements of Terray *et al.* [40] were in strongly-forced fetch-limited waves, whereas those of Drennan *et al.* [41] represent fully-developed sea with an almost infinite fetch (the Atlantic Ocean). Delvigne and Sweeney [42, p. 6] reported that  $\varepsilon$  varies between  $10^{-3}$  and  $10^{-2} \text{ m}^2/\text{s}^3$  for the surface layer and between 1 and  $10 \text{ m}^2/\text{s}^3$  for breaking waves. However, they do not define the “surface layer” nor did they explain the type of wave breaker. It appears therefore, that additional studies are needed to quantify and define  $\varepsilon$  at sea. But the flexibility in obtaining high values of  $\varepsilon$  in the BF makes using it preferable to using the SF.

The use of an average value of  $\varepsilon$  is probably more plausible for the BF than for the SF; when one uses a spatially averaged value, such as  $\bar{\varepsilon}$ , as representative of the mixing regime, it is preferable that the spatial distribution does not follow a pattern. The mixing in the SF at high rpm is axi-symmetric with a quasi-stagnant core (Figures 3 and 8). In essence, there are two zones with different mixing characteristics. A spatial average might not have much physical significance in such a case. The velocities (and subsequently the local  $\varepsilon$  values) in the BF (Figures 4 and 9) were distributed more evenly throughout the flask, such that a clear pattern did not exist. Thus, using an average value of  $\varepsilon$  to represent the mixing in the flask is more meaningful.

## 6. Conclusions

The velocities and energy dissipation rates in two eccentrically rotated flasks were evaluated using a HWA. The flasks are the Swirling Flask (SF), Figure 1a, a standard Erlenmeyer flask, and another that contains baffles in it, and is thus designated the Baffled Flask (BF), Figure 1b. Five rotation speeds of the orbital shaker were considered and they were  $\Omega = 50, 100, 150, 175$  and  $200$  rpm. The radial and azimuthal speeds were measured for each  $\Omega$ , and used to evaluate the overall water motion and to quantify turbulence characteristics in each flask. It was found that the flow in the SF is in general two-dimensional changing from horizontal at low  $\Omega$  and to axi-symmetric at high  $\Omega$  (Figure 3). The flow in the BF appeared to be three-dimensional at all  $\Omega$  (when the results of Figure 4 are used along with visual observation). The average speed in the SF increased slowly with  $\Omega$  while that in the BF increased sharply when  $\Omega$  reached 150 rpm and above. The spectra of the SF speeds were dominated by periodicity at all  $\Omega$  while those of the BF manifested a decrease in periodicity as  $\Omega$  was increased. The energy dissipation rate,  $\varepsilon$ , in the SF decreased sharply with depth while that in the BF was uniformly distributed throughout the flask.

The flask-averaged  $\varepsilon$  in both flasks was practically the same for  $\Omega$  smaller than or equal to 100 rpm. For higher values of  $\Omega$ ,  $\varepsilon$  of the SF was in general two orders of magnitude smaller than that in the BF. For  $\Omega \geq 150$  rpm, the Kolmogorov scale in the SF was about five times larger than that in the BF. In particular, the sizes of the Kolmogorov scale in the BF at  $\Omega \geq 150$  rpm approached the size of oil droplets observed at sea, which is 50–400  $\mu$  [8, 10, 20, 38, 39]. Based on the observed three-dimensional motion, and the Kolmogorov scale, it appears that the BF is more representative of mixing at sea due to breaking waves than the SF.

### Acknowledgement

This research was supported, in part, by the U.S. Environmental Protection Agency through Contract No. PR-OH-01-00381. However, no official endorsement of the results should be implied.

### References

1. Taylor, G.I.: 1953, Dispersion of soluble matter in solvent flowing slowly through a tube, *Proc. R. Soc. Lon. Ser. A.* **219**, 186–203.
2. Taylor, G.I.: 1954, The dispersion of matter in turbulent flow through a pipe, *Proc. R. Soc. London Ser. A.* **223**, 446–468.
3. Fischer, H.B., List, E.J., Koh, R., Imberger, J. and Brooks, N.H.: 1979, *Mixing In Inland and Coastal Waters*, Academic Press, New York, NY.
4. Clayton, J.R., Payne, J.R. and Farlow, J.S.: 1993, *Oil Spill Dispersants, Mechanical Action and Laboratory Tests*, Boca Raton, C. K. Smoley, Florida.
5. Fingas, M.F., Hughes, K.A. and Schweitzer, M.A.: 1987, Dispersant testing at the Environmental Emergencies Technology Division, *Proc. Tenth Arctic Marine Oil Spill Program Technical Seminar*, Conservation and Protection, Canada, pp. 343–356.
6. Fingas, M.F.: 1991, Dispersants: A Review of Effectiveness Measures and Laboratory Physical Studies, *Proc. Alaska RRT Dispersant Workshop, U.S. Minerals Management Service*, Anchorage, Alaska, p. 37.
7. Fingas, M.F.: 2000, Use of surfactants for environmental applications, In: Laurier L. Schramm (ed.), *Surfactants: Fundamentals and Applications to the Petroleum Industry*, pp. 461–539, Chap. 12, Cambridge University Press, Cambridge, UK.
8. Byford, D.C. and Green, P.J.: 1984, A view of the Mackay and Labofina laboratory tests for assessing dispersant effectiveness with regard to performance at sea, In: T.E. Allen (ed.), *Oil Spill Chemical Dispersants: Research, Experience, and Recommendations*, pp. 69–86, American Society of Testing and Materials, STP 840, Philadelphia, PA.
9. Martinelli, F.N.: 1984, The Status of warren spring laboratory's rolling flask test, In: T. E. Allen (ed.), *Oil Spill Chemical Dispersants, Research Experience and Recommendations*, pp. 55–68, American Society of Testing and Materials, STP 840, Philadelphia, PA.
10. Lunel, T.: 1993, Dispersion: Oil drop size measurements at sea, *Proc. 16th Arctic and Marine Oil Spill Program*, Canada, pp. 1023–1057.
11. Lunel, T. and Davies, L.: 1996, Dispersant effectiveness in the field on fresh oils and emulsions, *Proc. 1996 Arctic and Marine Oil Spill Program (AMOP)*, Canada, pp. 1355–1394.

12. Nordvik, A., Hudon, T. and Osborn, H.: 1993, Inter-laboratory calibration testing of dispersant effectiveness, Marine Spill Response Corporation Technical Report, Series 93-003, Washington, D. C.
13. Fiocco, R.J., Daling, P.S., DeMarco, G., Lessard, R.R. and Canevari, G.P.: 1999, Chemical dispersibility study of heavy bunker fuel oil, *Proc. 22nd Arctic Marine Oil Spill Program Technical Seminar*, Environment Canada, Ottawa, ON, pp. 173-186.
14. Canevari, G.P., Calcavecchio, P., Lessard, R.R., Becker, K.W. and Fiocco, R.J.: 2001, Key parameters affecting the dispersion of viscous oil, *Proc. 2001 Int. Oil Spill Conf., American Petroleum Institute*, Washington, DC, pp. 479-483.
15. Sorial, G.A., Venosa, A.D., Koran, K.M., Holder, E. and King, D.W.: 2004, Oil spill dispersant effectiveness protocol. I: Impact of operational variables, *J. Environ. Eng.* **130**(10), 1073-1084.
16. Sorial, G.A., Venosa, A.D., Koran, K.M., Holder, E. and King, D.W.: 2004, Oil spill dispersant effectiveness protocol. II: Performance of revised protocol, *J. Environ. Eng.* **130**(10), 1085-1093.
17. Chandrasekar, S., Sorial, G.A. and Weaver, J.W.: 2005, Dispersant effectiveness on three oils under various simulated environmental conditions, *Envir. Eng. Sci.* **22**(3), 324-336.
18. Kolmogorov, A.N.: 1941, The local structure of turbulence in incompressible viscous fluid for very large Reynolds number, *Dokl. Akad. Nauk. SSSR* **30**, 301-305. Reprinted in 1991: *Proc. R. Soc. Lond. A*, **434**, 9-13.
19. Nelkin, M.: 1994, Universality and scaling in fully developed turbulence, *Adv. Phys.* **43**(2), 143-181.
20. Delvigne, G.A.L., van der Stel, J.A. and Sweeney, C.E.: 1987, Measurement of vertical turbulent dispersion and diffusion of oil droplets and oiled particles, Report No. Z75-2, Delft Hydraulics Laboratory, Delft, The Netherlands.
21. Camp, T.R. and Stein, P.C.: 1943, Velocity gradient and internal work in fluid motion, *J. Boston Soc. Civ. Eng.* **30**(4), 219-237.
22. Tennekes, H. and Lumley, J.L.: 1972, *A First Course in Turbulence*, Chap. 3, MIT Press, Cambridge, MA.
23. Stanley, S.J. and Smith, D.W.: 1995, Measurement of turbulent flow in standard jar test apparatus, *J. Environ. Eng.* **121**(12), 902-910.
24. Cheng, C.-Y., Atkinson, J.F. and Bursik, M.I.: 1997, Direct measurement of turbulence structures in mixing jar using PIV, *J. Environ. Eng.* **123**(2), 115-125.
25. Batchelor, G.K.: 1970, *The Theory of Homogeneous Turbulence*, The University Press, Cambridge, p. 104.
26. Hinze, J.O.: 1987, *Turbulence, An Introduction to its Mechanisms and Theory*, 2nd ed., McGraw Hill Classic Textbook Reissue, McGraw-Hill, New York, N.Y., p. 41.
27. Kolmogorov, A.N.: 1962, A refinement of previous hypotheses concerning the local structure of turbulence in a viscous incompressible fluid at high Reynolds number, *J. Fluid Mech.* **13**, 82-85.
28. Rao, M.A. and Brodkey, R.S.: 1972, Continuous flow stirred tank turbulence parameters in the impeller stream, *Chem. Eng. Sci.* **27**, 137-156.
29. Wu, H. and Patterson, G.K.: 1989, Laser doppler measurements of turbulent flow parameters in a stirred mixer, *Chem. Eng. Sci.* **44**, 2207-2221.
30. Kaku, V.J., Boufadel, M.C. and Venosa, A.D.: 2002, Evaluation of Mixing Energy in the Swirling and Baffled Flasks, *Proc. Oil Spill Conf.*, Rhodes, Greece, Wessex Institute of Technology, pp. 211-218.

31. Kresta, S.M. and Wood, P.E.: 1993, The flow field produced by a pitched blade turbine: Characterization of the turbulence and estimation of the dissipation rate, *Chem. Eng. Sci.* **48**(10), 1761–1774.
32. Wu, H., Patterson, G.K. and van Doorn, M.: 1989, Distribution of turbulence energy dissipation rates in a rushton turbine stirred mixer, *Exp. Fluids* **8**, 153–160.
33. Pinton, J.-F. and Labbé, R.: 1994, Correction to the Taylor hypothesis in swirling flows, *J. Phys. II France* **4**(9), 1461–1468.
34. Monin, A.S. and Yaglom, A.M.: 1975, *Statistical Fluid Mechanics: Mechanics of Turbulence*, Vol. 2, MIT Press, Cambridge, Massachusetts, p. 11.
35. Kaku, V.J., Boufadel, M.C. and Venosa, A.D.: 2006, Evaluation of mixing energy in laboratory flasks used for dispersant effectiveness testing, *J. Environ. Eng.* **132**(1), 93–101.
36. Kitaigorodskii, S.A., Donelan, M.A., Lumley, J.L. and Terray, E.A.: 1983, Wave-turbulence interactions in the upper ocean. Part II: Statistical characteristics of wave and turbulent components of the random velocity field in the marine surface layer, *J. Phys. Oceanogr.* **13**, 1988–1999.
37. Kreyszig, E.: 1999, *Advanced Engineering Mathematics*, Chap. 17, 8th ed., John Wiley & Sons, New York, N. Y.
38. Delvigne, G.A.L.: 1983, Sea measurements on natural and chemical dispersion of oil, Report No. M1933-I, Delft Hydraulics Laboratory, Delft, The Netherlands.
39. Mackay, D., Chau, A. and Poon, Y.C.: 1986, A study of the mechanism of chemical dispersion of oil spills, Publication EE-76, Environmental Protection Agency, Ottawa, p. 150.
40. Terray, E.A., Donelan, M.A., Agrawal, Y.C., Drennan, W.M., Kahma, K.K., Williams III A.J., Hwang, P.A. and Kitaigorodskii, S.A.: 1996, Estimates of kinetic energy dissipation under breaking waves, *J. Phys. Oceanogr.* **26**, 792–807.
41. Drennan, W.M., Donelan, M.A., Terray, E.A. and Katsaros, K.B.: 1996, Oceanic turbulence dissipation measurements in SWADE, *J. Phys. Oceanogr.* **26**, 808–815.
42. Delvigne, G.A.L. and Sweeney, C.E.: 1988, Natural dispersion of oil, *Oil Chem. Pollut.* **4**, 281–310.